Pol. J. Environ. Stud. Vol. 31, No. 6 (2022), 1-12
DOI: *10.15244/pjoes/151865* ONLINE PUBLICATION DATE:

Original Research

Adsorption of Iodine from Aqueous Solution on Modified Silica Gel with Cyclodextrin Derivatives

Badr Al-Fulaiti, El Said I. El-Shafey, Salim Habib Salim Al Kindi, Raid J. Abdel-Jalil*

Chemistry Department, College of Science, P.O. Box 36, Sultan Qaboos University, PC 123, Muscat, Oman

Received: 11 March 2022
Accepted: 4 July 2022

Abstract

The presence of excessive amount of iodine, especially radioactive iodine is dangerous in the environment. The aim of this research is to prepare functionalized silica with cyclodextrin with different hydrophobic cavity sizes to investigate their performance in iodine adsorption. Cyclodextrin (CD) derivatives (αCD, βCD, γCD and hp-βCD) were successfully immobilized on silica gel surface via epichlorohydrin as a cross linker. The ratio of silica (Si) to CD was optimized in preliminary experiments based on the highest uptake of iodine. Selected adsorbents with varied ratios of silica to CD derivatives are investigated, including Si-αCD (3:2), Si-βCD (4:1), Si-γCD (4:1) and Si-hp-βCD (4:1). The adsorption of iodine (I_2/KI) solution was investigated in terms of initial pH, contact time, iodine concentration and temperature. No significant variations was noticed for iodine adsorption at different pH values, thus, initial pH 6 was selected for further studies. Equilibrium adsorption was reached faster on Si-hp-bCD than other adsorbents with kinetic adsorption data fitting well pseudo second order model. Activation energy (E_a) was found to be in the range of 12.7-23.4 kJ/mol. Equilibrium adsorption data were found to fit well the Langmuir adsorption model with lower uptake as temperature rises. Iodine uptake follows the order: Si-hp-βCD (714 mg/g) >Si-αCD (625 mg/g) >Si-βCD (555.6 mg/g)> Si-γCD (435 mg/g). Thermodynamic study showed that iodine adsorption is exothermic and spontaneous. Adsorbents' reuse exhibited excellent performance for iodine adsorption with a decrease in iodine uptake of ~2-4% in the third adsorption cycle. The study shows that the functionalized silica with hp-bCD shows best performance in terms of kinetics and equilibrium.

Keywords: adsorption, iodine, silica, cyclodextrin, functionalization, epichlorohydrin

*e-mail: jalil@squ.edu.om

Introduction

Nuclear energy is one of the most reliable sources of energy that is highly efficient without emissions of carbon dioxide. It can solve the problems of energy shortages and environmental pollution if properly maintained without severe earthquakes. The emissions from nuclear power plants include significant amounts of I^{131} and I^{129} isotopes with half-life times of 8.02 days and 1.57 $x10^7$ years, respectively [1, 2]. Radioactive I^{131} is used for the treatment of hyperthyroidism, a medical condition of an overactive thyroid, while I^{129} is mostly released in the environment form nuclear weapons testing. Different industries participate in iodine discharge in the environment including food, chemical and pharmaceutical industries [3]. Groundwater and surface water can be contaminated by the discharge of iodine – contaminated wastewater [4]. Iodine pollution currently receives a growing concern due to its high toxicity to the thyroid glands in humans and animals [5]. Excessive amounts of iodine can cause hypothyroidism [6] and is linked to autoimmune thyroiditis in humans and animals [7], Thus, efficient removal of iodine from environment is necessary regardless of its challenge. Different adsorbents have been used for the removal of iodine from aqueous solutions including activated carbon [8], metal-exchanged zeolite [9], porous copper-doped silica zeolites [10], graphene [11], aerogel [12], metal-organic framework (MOF) [13], and porous organic polymer materials [14]. MOFs showed high uptake of iodine, however, they are unsuitable because of their instability in aqueous or humidity conditions [2]. Inorganic adsorbents have been used for iodide removal such as Bismuth based adsorbents [15], and porous polymer microspheres from lignin-derived phenols [16].

Cyclodextrin (CD), a representative of cyclic oligosaccharide macromolecules, is non-toxic material in addition of being green and biodegradable. CD structure consists of a hydrophilic exterior and a hydrophobic inner cavity [17, 18]. Such unique cavity allows CD to contain pollutants via the formation of "host-guest" encapsulated-inclusion complexes with those pollutants [18-20]. Cyclodextrins are basically 3 types α-, β- and γ-cyclodextrins having six, seven, or eight glucose units, linked with α-1,4-glycosidic bonds, respectively [18]. Cyclodextrins form inclusion complexes with iodine [18-20].

In this research, epichlorohydrin (EPI) was used as a crosslinking agent to bind αCD, βCD, γCD and hydroxyl propyl beta cyclodextrin (hp-βCD) onto silica gel surface. Silica gel has beneficial mechanical and chemical properties as it is is easy to functionalize. Thus is the most commonly used support for bonded phase chromatography [21]. Produced adsorbents were tested for the adsorption of iodine from aqueous solutions in terms of kinetics and equilibrium. In this research, the effect of the different sizes of the hydrophobic cavity of CD in iodine inclusion via hydrophobic interaction forces [22], will be investigated.

Materials and Methods

Materials

All chemicals used were of analytical grade. Silica gel was purchased from sigma Aldrich and was dried at 65ºC for 24 hours prior to use. All cyclodextrins used in this study were purchased from cyclolab company. A Stock solution of 7 g/L of iodine was prepared by dissolving 15 g of KI and 7 g of I_2 in 1 L of deionized water. Other iodine concentrations were prepared by suitable dilution in deionized water.

Adsorbent Preparation and Characterization

General Procedure for the Preparation of the Cyclodextrin Modified Silica Gel

Preparation of β-cyclodextrin cross liked with silica polymer:

In a typical procedure: a respective CD (2.50 g) and silica gel (2.50 g) were dissolved in a solution of sodium hydroxide (10.0 g) in distilled water (10.0 ml). The aqueous solution was stirred at room temperature using mechanical stirring for 30 min.

Epichlorohydrine was then added drop wise over a period of one hour with continuous stirring. The solution was then heated to 65ºC for 3 hours. After cooling to room temperature, acetone (10.0 ml) was added and the resultant solution was stirred at room temperature overnight. The insoluble polymer was collected by suction filtration and the solid obtained was washed several times with distilled water (50 ml x 5) and acetone (50 ml x 5). The white solid thus obtained was kept for drying overnight n in oven at 55ºC.

Silica modification with different cyclodextrines (α, β, γ and β-hydroxypropyl-CD) was carried out using different mass ratios of silica to CD: 4:1, 3:2, 1:1, 2:3 and 1: 4, respectively following the same method mentioned above. A schematic representation of modified silica preparation is presented in Fig. 1. Based on preliminary experiments, the following adsorbents showed best performance of iodine sorption, with silica to cyclodextrin mass ratio of (3:2 α-CD), and (4:1 β-, γ- and hp-β-CD).

Adsorbent Physico-Chemical Characterization

The surface area of silica and modified silica adsorbents were determined via nitrogen adsorption at 77 K using ASAP 2020 instrument (Micrometrics, USA). Degassing was carried out at 55ºC under vacuum for 24 hours. Scanning electron microscopy (SEM) and energy dispersive spectroscopy (EDS) were carried out for the adsorbents at a 20 kV accelerating voltage using

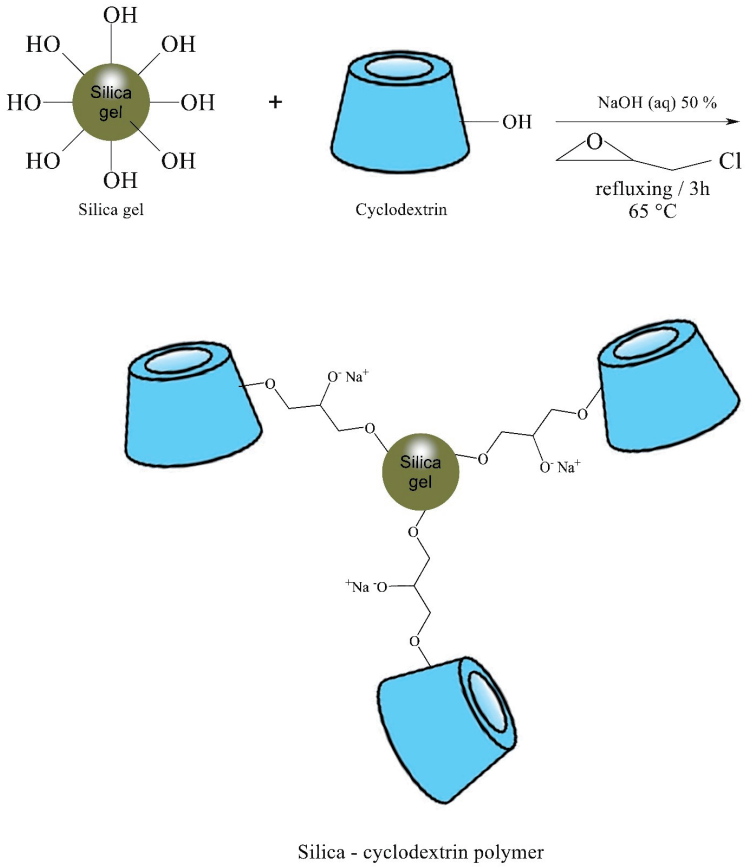

Fig. 1 A schematic representation of silica surface modification with cyclodextrin.

JEOL/EO JSM 5600 scanning electron microscope (Jeol, Japan) and a JEOL/O JSM 5600 editor energy disperse analysis system (Joel, Japan) that is fitted with the scanning microscope. Carbon powder was used in sample coating to render the substance conductive.

X-ray powder diffraction (XRD) was conducted using a Philips PW 1830 generator with a Philips PW 1050 powder goniometer (Philips, USA) and copper K_{α} as the incident radiation. FTIR was carried out using FT-IR spectrometer (Spectrum BX, Berkin Elmer, Germany). Zero point of charge (pH_{zpc}) was carried out following Moreno-castilla et al. method [23] and apparent density was evaluated using a standard method [24]. Thermogravimetric analysis (TGA) was tested using SDT Q600 Simultaneous DSC-TGA equipment (TA instruments, USA). Heating was carried out under nitrogen with a flow rate of 100 mL/min from room temperature to 700°C at a heating rate of 10°C/min.

Adsorption of Iodine from Aqueous Solution

Based on preliminary work using modified silica at different silica-CD ratios, best uptake of iodine was found to be on Si-αCD (3:2), Si-βCD (4:1), Si-γCD (4:1) and Si-hp-βCD (4:1). Accordingly, these adsorbents were selected for the iodine adsorption study.

Effect of Initial pH

In this experiment, 0.1 g of each adsorbent was mixed with 25 mL of iodine solutions (500 mg/L) at different initial pH values (3.0-6.0) at room temperature (25°C). Prior to adsorbent mixing with iodine solution, the pH was adjusted using drops of 0.1 M HCl or 0.1 M NaOH. The adsorption mixture was kept under agitation until the equilibrium was reached. Residual iodine solutions were separated and analyzed spectrophotometrically at λmax of 288 nm using varian/Cary/50 Conc UV-visible spectrophotometer (USA). From this study, initial pH 6 was found optimal and thus was selected for further kinetic and equilibrium studies.

Kinetics of Iodine Adsorption

The kinetic experiments were conducted by mixing 0.2 g of each adsorbent to iodine solutions (50 mL, 500 mg/L) at room temperature (25°C) and pH 6. The sorption mixture was kept under mechanical agitation. At different periods of time, aliquots of supernatant were withdrawn and analyzed for iodine content. The experiment was repeated at 35°C. An iodine sample with the same initial concentration and pH was kept under the same experimental conditions as a reference.

Equilibrium Studies

~0.1 g of each adsorbent was mixed with 25 mL of iodine (200-5000) mg/L at initial pH 6 and 25ºC. The adsorption mixtures were left under mechanical agitation until the equilibrium was reached. Aliquots of supernatant of iodine solution were withdrawn for analysis. The experiment was repeated at 35ºC.

Adsorbent Reuse for Iodine Adsorption

0.3 g of each adsorbent were mixed with iodine solutions (50 mL, 1000 mg/L) at pH 6 and room temperature. After the equilibrium was reached, the adsorption mixture was filtered, and a sample of the filtrate was separated for analysis. The adsorbent residue was impregnated in NaOH (30 mL, 0.5 M) for 10 minutes for iodine desorption. The adsorbents, afterwards, were washed with deionized water to remove residual basicity and was partially dried at room temperature. The adsorbents were carefully transferred to a fresh iodine solution with the same conditions as in the first adsorption cycle above. Three consecutive adsorption cycles were carried out in this study. All experiments and analysis were carried out at least twice.

Results and Discussion

Physico-Chemical Characterization of Adsorbents

Surface area and surface porosity were determined, Table 1, via nitrogen adsorption-desorption isotherms at 77 K. The surface area of silica was 428 m^2/g, however, on functionalization, the surface area has tremendously decreased. Silica and modified silica show mesoporous structure domination in terms of mesoporous surface area (S_{meso}) and average pore diameter (D). CD immobilization on silica surface has occupied the surface limiting the access for nitrogen adsorption, and thus, decreasing the surface area tremendously [25].

Fig. 2 shows SEM micrographs of silica gel and selected modified silica gel Si-αCD (3:2), Si-βCD (4:1), Si-γCD (4:1) and Si-hp-βCD (4:1). SEM micrographs of functionalized silica appears different from original silica due to CD immobilization. The surface is generally heterogeneous without homogenous distribution. As a limitation of the technique, SEM micrographs usually vary depending on sections chosen for the micrograph, particularly for heterogeneous surfaces [25].

EDS analysis, Table 2 (Fig. 1a, Appendix) shows ~10% of carbon on silica. This is because of using carbon powder as coating on the adsorbent surface to keep the surface conductive. On CD immobilization, the carbon content increased (60-65%) while oxygen content (34-37%) decreased. Silicon content has tremendously decreased on CD immobilization, and this is because the silicon particles was covered by the cross-linker and immobilized CD while EDS electron beam penetrates from 100 nm to 1 μm depth on the surface [26]. EDS, as a technique, shows some limitations. Detection and quantification of light elements with atomic numbers <11 is difficult as x-rays produced by these light elements are difficult to separate from background and superposition [27]. X-rays produced from the specimen atoms are emitted in all directions and some of these x-rays may not escape the sample and, thus, some elements might not be detected [25].

The apparent density, Table 2, shows that silica has higher density than functionalized silica. Immobilized CD derivatives via the crosslinker has led to an increase in particle size with less added mass. Consequently, modified silica possesses a decreased apparent density. The variation of surface pH_{zpc} appears insignificant for silica and functionalized silica (Table 2).

The XRD pattern of Silica shows a peak at 2θ of 23° that corresponds with amorphous silica [25]. However, on functionalization, a shift of that peak to lower 2θ value of ~20° took place (Fig. 3). Such variation is related to the structure alteration associatd with the incorporation of CD derivatives on silica surface [28, 29].

FTIR spectra of carbons are presented in Fig. 4. The band at ~3370 cm^{-1} for functionalized silica corresponds with O-H stretching vibration. Such band is not available on silica spectrum. The shoulder and band that appear for modified silica at 2910 and 2870 cm^{-1} are related to C-H asymmetric and symmetric stretching vibration in $-CH_2$ group, respectively. Such shoulder and band are not available on silica gel surface. The presence

Table 1. Surface texture of silica and CD modified silica.

Sorbent	BET Surface area (m^2/g)	V_t (ml/g)	D (A°)	Mesopore area (m^2/g)	Micropore area (m^2/g)	V_{micro} (ml/g)	V_{meso} (ml/g)
Silica	428.3	0.784	73.2	417.1	11.1	0.005	0.778
Si-aCD (3:2)	5.98	0.008	53.3	4.61	1.36	0.0002	0.008
Si-bCD (4:1)	5.07	0.005	39.2	3.74	1.33	0.0003	0.005
Si-gCD (4:1)	6.32	0.007	43.3	3.95	2.37	0.0001	0.007
Si-hp-bCD (4:1)	8.45	0.010	47.8	4.75	3.70	0.00008	0.010

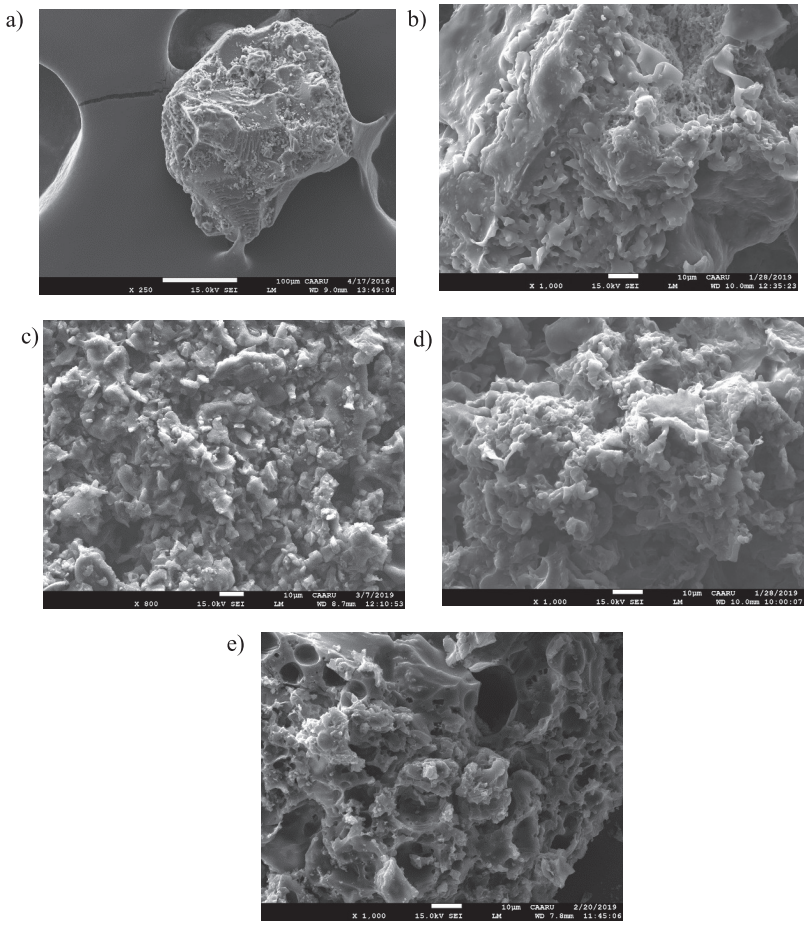

Fig. 2. SEM micrographs of a) silica gel, b) Si-αCD, c) Si-βCD, d) Si-γCD e) Si-hp-βCD.

of the above-mentioned bands on functionalization reflects a successful immobilization of CDs on modified silica. The band at 1640 cm^{-1}, is related to C=C or C=O vibration in αCD and βCD immobilized. Probably, this results from a degree of EPI polymerization [30]. The band at 1455 cm^{-1}, is mostly related to C-H pending vibrations on functionalized silica. Such band is not available for silica (Fig. 4). The bands between 1320–1000 cm^{-1} are related to O−H bending and C−O stretching vibrations in ether structure. The band at 1059 cm-1 on silica and modified silica can be related to Si-O-Si vibration [31]. Finally, the band at 850 cm^{-1} is related to Si-O vibration.

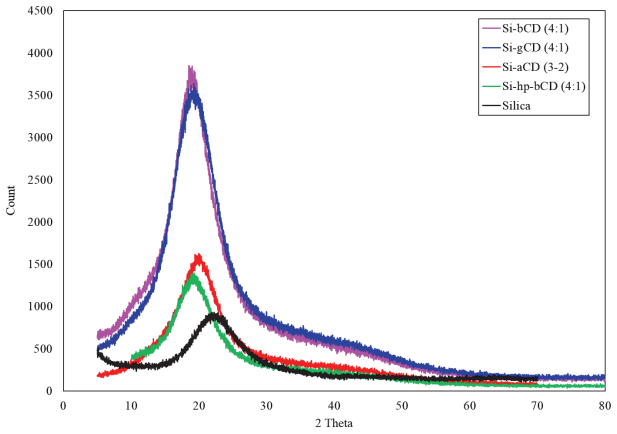

Fig. 3. X-ray diffraction of silica and modified silica.

Table 2. Surface texture of silica and CD modified silica.

Sorbent	BET Surface area (m^2/g)	V_t (ml/g)	D (A°)	Mesopore area (m^2/g)	Micropore area (m^2/g)	V_{micro} (ml/g)	V_{meso} (ml/g)
Silica	428.3	0.784	73.2	417.1	11.1	0.005	0.778
Si-aCD (3:2)	5.98	0.008	53.3	4.61	1.36	0.0002	0.008
Si-bCD (4:1)	5.07	0.005	39.2	3.74	1.33	0.0003	0.005
Si-gCD (4:1)	6.32	0.007	43.3	3.95	2.37	0.0001	0.007
Si-hp-bCD (4:1)	8.45	0.010	47.8	4.75	3.70	0.00008	0.010

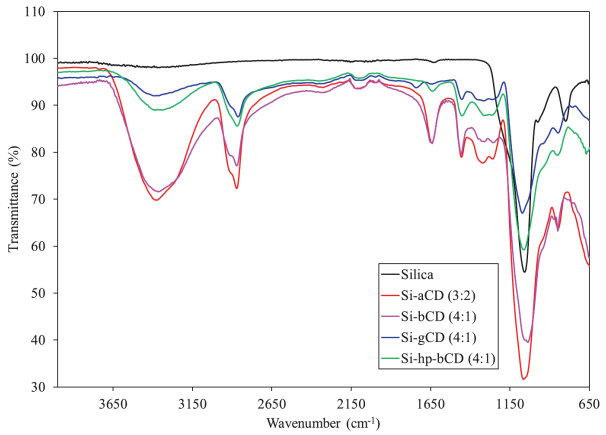

Fig. 4. FTIR spectra of silica and modified silica.

Thermogravimetric analysis (TGA) of silica and functionalized silica are presented in Fig. 5a). In the early stage of thermal decomposition of adsorbents from room temperature to 150ºC, weight loss is related to the loss of moisture. The moisture weight loss corresponds to ~2.2% for silica however for functionalized silica moisture ranges between 7.9 to 8.8% (Fig. 5b). This is due to the immobilized CD which possesses large content of -OH groups that adsorb water vapor via H-bonding. In the second stage of thermal decomposition between 150-800ºC, the weight loss is related to volatiles that breaks away from the surface. Silica does not show further thermal decomposition with temperature rise with insignificant weight loss. However, functionalized silica shows tremendous loss of weight on temperature rise. Maximum weight loss for functionalized silica took place between 300 and 400ºC which corresponding to weight loss of 86.7, 73.9, 77.6 and 85.1% for Si-αCD, Si-βCD, Si-γCD and Si-hp-βCD, respectively. This reflects the chemical bonding nature of CD on silica surface. In this range of temperature, both CO_2 and CO break away as volatiles

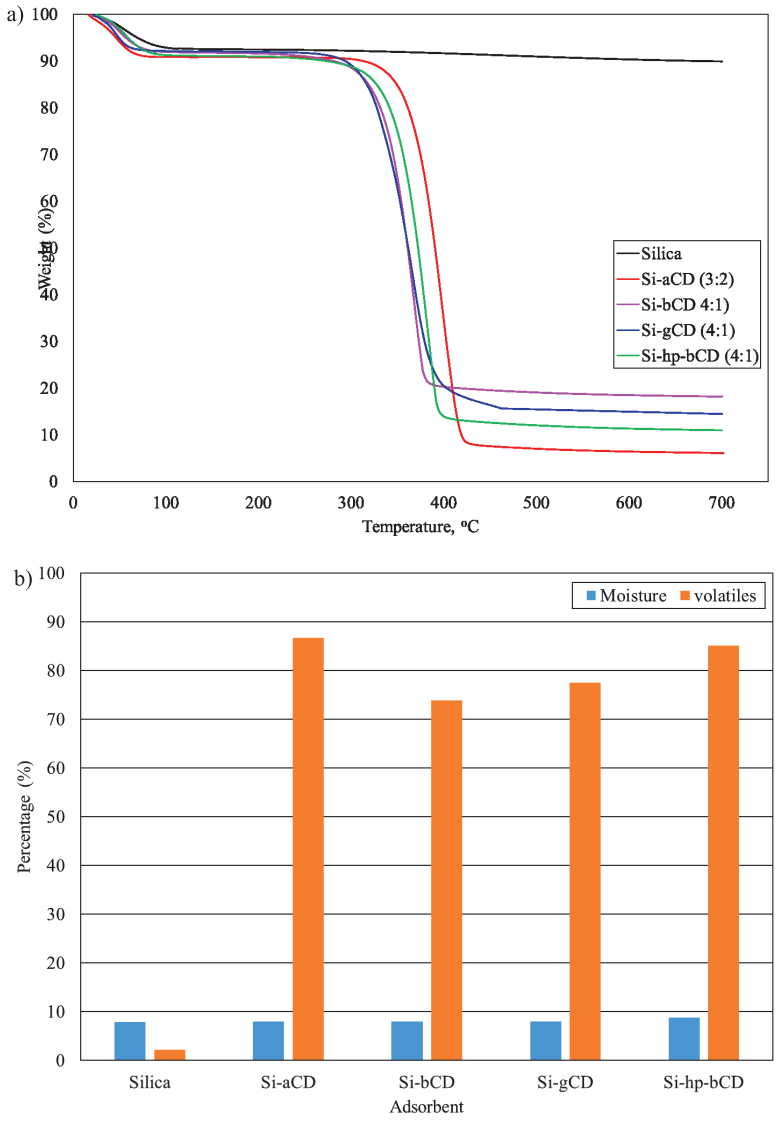

Fig. 5. a) TGA od silica and modified silica, b) percentage of weight loss of moisture and volatiles from silica and modified silica.

[32]. The high amount of volatiles that break away from modified silica, at such high temperature, reflects the larger amount of CD immobilized on silica surface.

Adsorption of Iodine

Effect of pH

The amount of adsorbed iodine (q_e) left at equilibrium is calculated from Eq. (1).

$$q_e = (C_o - C_e)V/m \quad (1)$$

where q_e (mg/g) is amount adsorbed at equilibrium, C_o and C_e are the initial concentration of iodine and at equilibrium, respectively. m is the mass of adsorbent in gram (g). Surface pH_{zpc} (zero point of charge) is the pH value at which surface charge is zero. At pH < adsorbent pH_{zpc}, the surface remains positively charged while at pH values higher than pH_{zpc}, the surface becomes negatively charged. The effect of initial pH values on iodine adsorption is presented in Fig. 6. It is clear that iodine adsorption shows insignificant variation with initial pH change. As presented in Fig. 7, the final pH ranges between pH 3.4-6.4 for all adsorbents. In solution, I_2, I^- and I_3^- exist in solution. It is expected that I_2 molecules are adsorbed on the hydrophobic chains and in CD hydrophobic cavities [33]. Charged species of I^- and I_3^- are not expected to be significantly adsorbed on modified silica surface. In previous studies on activated carbon, it was concluded that only I_2 is adsorbed while I^- or I_3^- are not [34, 35]. Adsorption of iodine follows the order: Si-hp-bCD > Si-aCD > Si-bCD > Si-gCD. This is probably because of increased hydrophobic sites of Si-hp-βCD due to the extended chain.

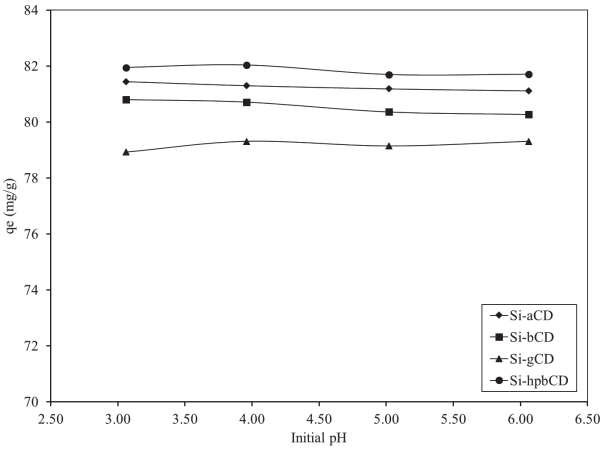

Fig. 6. Effect of initial pH on iodine adsorption.

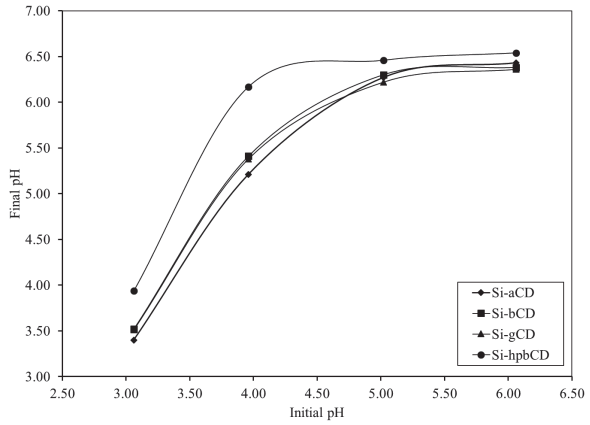

Fig. 7. Equilibrium pH vs initial pH.

Kinetics of Iodine Adsorption

Iodine adsorption was found fast reaching equilibrium in approximately 2 hours for Si-γCD, Si-αXD and Si-hp-βCD while, for Si-βCD it requires more time of ~4 hours (Fig. 8).

Iodine uptake was found to vary almost linearly $(time)^{0.5}$ in the early stages of iodine adsorption, Eq. (2) [36].

$$q_t = k_d\, t^{0.5} \quad (2)$$

where q_t is the quantity of iodine adsorbed per g of adsorbent (mg/g) at time t while k_d is the diffusion constant. The adsorption kinetic data were tested for both pseudo first-order and second-order kinetic models (Eq. 3-4) [37].

$$Log(q_e - q_t) = log\, q_e - k_1 t/2.303 \quad (3)$$

$$t/q_t = 1/k_2 q_e^2 + t/q_e \quad (4)$$

k_1 and k_2 are rate constants for pseudo first order model and pseudo second order model, respectively. The initial adsorption rate, h, was calculated from Eq. (5) [37].

$$h = k_2 q_e^2 \quad (5)$$

As presented in Table 3, the adsorption kinetic data fit well pseudo second order kinetic model than pseudo first order model as indicated by their respective R^2 values. Such a good fitting for pseudo second order kinetic model indicates that iodine adsorption rate depends on both the adsorbate concentration and the adsorption sites on the adsorbent suggesting a mechanism of sharing or electron sharing between the modified silica surface and iodine molecules [37]. Because of the low R^2 values accompanied the application of pseudo first order model to the kinetic data, the kinetic parameters of the model are not discussed. In a previous study [38], iodine adsorption kinetic data on a microporous polymer were found to fit well pseudo second order kinetic model.

Rising the temperature showed an increase in the values of k_d and k_2 for all adsorbents tested unlike q_e as it shows a decrease on temperature rise. Since h

Table 3. Kinetics parameters for iodine adsorption on modified silica at 25 and 35ºC.

Sorbent	Temp.	Pore diffusion constant, k_d (mg/g/min$^{0.5}$)	Pseudo first order model			Pseudo second order model			E_a (kJ/mol)
			k_1 (min^{-1})	q_e (mg/g)	R^2	Rate const k_2, (g/mg/min)	Initial adsorption rate, h, (mg/g/min)	Monolayer, q_e, (mg/g)	R^2	
Si-αCD	25ºC	13.00	0.034	139.8	0.9465	0.0003	4.656	120.5	0.9992	18.02
	35ºC	11.76	0.018	66.6	0.9900	0.0004	3.547	93.5	0.9993	
Si-βCD	25ºC	7.09	0.010	96.0	0.9911	0.0001	1.998	123.5	0.9998	23.36
	35ºC	7.39	0.014	77.5	0.9972	0.0002	1.816	101.0	0.9991	
Si-γCD	25ºC	11.70	0.007	43.9	0.6516	0.0002	4.713	119.1	0.9999	14.24
	35ºC	12.43	0.015	12.4	0.4200	0.0003	3.500	93.5	0.9998	
Si-hp-βCD	25ºC	14.18	0.040	164.5	0.9325	0.0004	6.353	125.0	0.9991	12.54
	35ºC	14.92	0.017	34.4	0.7637	0.0005	5.200	104.2	0.9998	

Fig. 8. Kinetics of adsorption of iodine at a) 25ºC and b) 35ºC on modified silica.

is directly proportional to q_e^2, it shows also a decrease on temperature rise. In general, the values of k_d, k_2, h and q_e follow the order: Si-hp-βCD > Si-αCD ≈Si-γCD >Si-βCD with a slight increase for k_2 value for S-αCD than Si-γCD at room temperature. Since q_e decreases on temperature rise, the adsorption process of iodine is considered exothermic process.

Due to the good fitting of pseudo second order model to the adsorption kinetic data, k_2 was utilized to calculate the activation energy, E_a (kJ/mol), for iodine adsorption. E_a, was calculated from Arrhenius equation for two temperatures (Eq. 6).

$$\ln(k'_2/k_2) = (E_a/R)[(1/T_1) - (1/T_2)] \qquad (6)$$

where R is the gas constant (8.314 J/mol/K), k_2 is rate constant at T_1 (298 K) and k'_2 is the rate constant at T_2 (308 K).

If E_a is less than 42 Kj/mol, the adsorption process is considered as physical adsorption and if E_a exceeds 42 kJ/mol, the process is considered as chemical adsorption process [39]. As shown in Table 3, E_a values were found to be in the range of 12.5-23.4 kJ/mol indicating that iodine adsorption process on these adsorbents is mainly physical and diffusion controlled process [39].

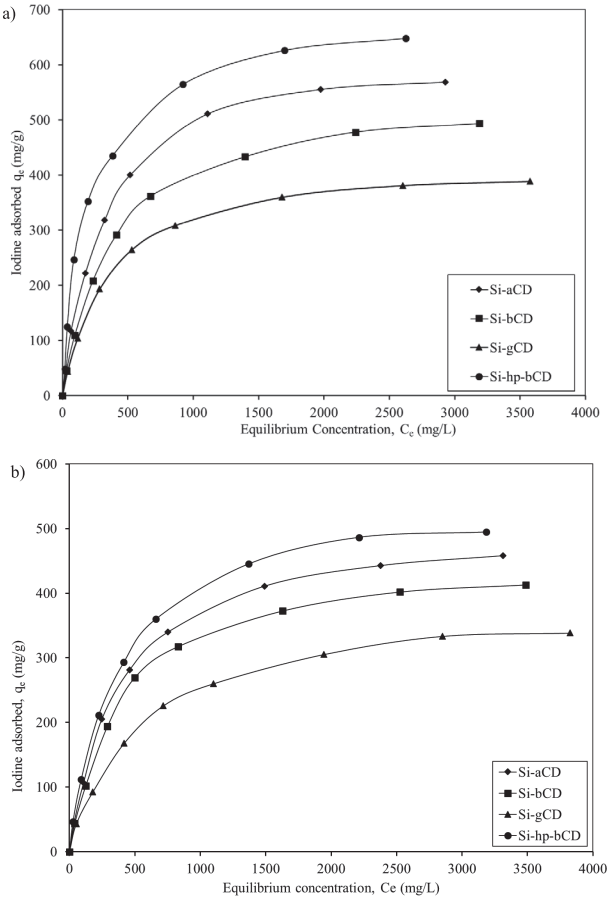

Fig. 9. Iodine adsorption isotherms at (A) 25ºC and b) 35ºC on modified silica.

Equilibrium Adsorption

Equilibrium adsorption was carried out at different iodine concentrations. As presented in Fig. 9, iodine uptake increases as concentration increases showing an L-type adsorption isotherm. The iodine adsorption was found to decrease on temperature rise from 25ºC to 35ºC. Both the Langmuir and the Freundlich isotherms (Eq. 7 and Eq. 8, respectively) were tested for the equilibrium adsorption data.

$$C_e/q_e = 1/b.q + C_e/q \quad (7)$$

$$\log q_e = 1/n(\log C_e) + \log K \quad (8)$$

where q and b are Langmuir constants associated with the monolayer adsorption capacity of iodine (mg/g) and Langmuir constant (L/mg), respectively. K ($L^{1/n}$ $mg^{1-1/n}$ /g) and $1/n$ are the Freundlich constants, related to adsorption capacity and adsorption intensity, respectively.

Langmuir isotherm shows better fitting to the equilibrium adsorption data showing high R2 values than the Freundlich isotherm model that shows low R^2 values (Table 4). Iodine adsorption process follows monolayer formation at equilibrium. An obvious decrease in iodine uptake with temperature rise from 25 to 35ºC (Fig. 9) showing an exothermic adsorption process on all adsorbents tested. The separation factor, R_s, shows values between 0 and 1 and this indicates a favorable adsorption [40].

The adsorption capacity of iodine was found to follow the order: Si-hp-βCD>Si-αCD>Si-βCD>Si-γCD.

Monolayer adsorption capacity (q) of iodine on modified silica in this study (Table 4) can be compared with different adsorbents from other studies. Iodine adsorption capacity on AC, prepared from spinach leaves with sulfuric acid activation, was 909 mg/g [41], on MOF (75.4 mg/g) [42], lignin based activated carbon (1206 mg/g) [4] and GO-chitosan sponge 30.5 mg/g [43].

Adsorption Thermodynamics of Iodine Adsorption

For iodine adsorption, the free energy change (ΔG^0), enthalpy change (ΔH^0) and entropy change (ΔS^0) can be calculated from the equilibrium constant, K_c, at different temperature. K_c can be calculated from Eq. (9). K_c was calculated from the initial linear part of the adsorption isotherm when q_e is plotted against C_e [25].

$$K_c = C_{Ae}/C_e \quad (9)$$

C_e is the equilibrium concentration of iodine (mg/L) and C_{Ae} is the amount of iodine adsorbed (mg/L). As shown in Table 5, K_c values decrease with temperature (Table 5). This reflects the exothermic nature of iodine. ΔG^0 was calculated as given in Eq. (10).

$$\Delta G^0 = -RT\ln K_c \quad (10)$$

ΔH^0 is calculated from Van't Hoff equation at two different temperatures (Eq. 11).

$$\ln(K_c'/K_c) = (\Delta H^o/R)(1/T_1-1/T_2) \quad (11)$$

where k_c and k_c' are the equilibrium constants at temperatures of T_1 and T_2 (Kelvin), respectively. The entropy change, ΔS^o, can be calculated from the values of ΔG^o and ΔH^o, as presented in Eq. (12).

$$\Delta G^o = \Delta H^0 - T\Delta S^0 \quad (12)$$

The negative values of ΔG^0 indicates a spontaneous process of iodine adsorption with more spontaneity on Si-hp-βCD. The negative ΔH^o values represents an exothermic nature of iodine adsorption. Similar results were found for iodine adsorption on MXene [44]. The negative values of ΔS^o indicates a decrease in the disorder on adsorption of iodine on adsorbents under investigation.

Table 4. Equilibrium parameters for iodine sorption at different temperature.

Sorbent	Sorption Temp. (ºC)	Langmuir constants		Separation factor, R_s	R^2	Freundlich constants		R^2
		q (mg/g)	*b* (L/mg)			*1/n*	*K*	
Si-αCD	25ºC	625.0	0.0033	0.04-0.60	0.9998	0.480	15.14	0.9308
	35ºC	497.5	0.0027	0.07-0.65	0.9994	0.502	10.19	0.9313
Si-βCD	25ºC	555.6	0.0027	0.06-0.65	0.9998	0.480	12.40	0.9254
	35ºC	454.6	0.0026	0.07-0.66	0.9996	0.498	9.26	0.9274
Si-γCD	25ºC	434.8	0.0029	0.05-0.63	0.9998	0.497	9.34	0.9548
	35ºC	384.6	0.002	0.09-0.72	0.9986	0.488	7.502	0.9381
Si-hp-βCD	25ºC	714.3	0.0049	0.03-0.50	0.9991	0.441	24.50	0.8988
	35ºC	555.6	0.0029	0.064-0.63	0.9993	0.494	12.10	0.9434

Table 5. Thermodynamic parameters for iodine adsorption on modified silica at 25 and 35ºC.

Sorbent	Temp.(*K*)	K_c	ΔG^o (kJ/mol)	ΔH^o(kJ/mol)	ΔS^o(J/mol)
Si-αCD	298	6.74	-4.73	-26.49	-73.0
	308	4.76	-3.87		-75.9
Si-βCD	298	5.45	-4.20	-23.80	-82.9
	308	3.99	-3.43		-86.0
Si-γCD	298	4.16	-3.53	-28.25	-73.9
	308	2.87	-2.61		-75.9
Si-hp-βCD	298	10.06	-5.72	-33.22	-92.3
	308	6.51	-4.64		-95.9

Adsorbents Reuse

As shown in Fig. 10, iodine adsorption in the third cycle showed a decrease of 2, 1.7, 3.8 and 1.5% on Si-αCD, Si-βCD, Si-γCD and Si-hp-βCD, respectively. It is clear that, the desorption process using 0.5 M of NaOH was very successful in this study.

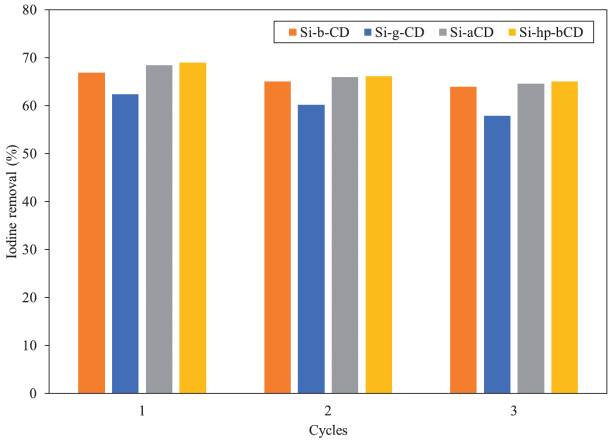

Fig. 10. Iodine adsorption recycle.

Conclusion

Silica surface modification with cyclodextrin using epichlorohydrin via chemical bonding was successful. The surface area of silica has tremendously decreased after surface functionalization. Initial pH shows almost no effect on iodine adsorption for all adsorbents. The process of iodine adsorption was found to follow well pseudo second order model. Si-hp-βCD shows the highest adsorption capacity at 25ºC (714 mg/g) while Si-γCD shows the lowest capacity of 435 mg/g. Thermodynamic study shows that the process of iodine adsorption is spontaneous and exothermic. Developed adsorbents in this study show excellent recyclability and reuse for iodine adsorption. In addition, It is expected that this adsorbent to have application in water purification from small organic and non-polar molecules.

Conflict of Interest

The authors declare no conflict of interest.

References

1. BANERJEE D., CHEN X., LOBANOV S.S., PLONKA A.M.X., CHAN. DALY J.A., KIM T., THALLAPALLY P.K., PARISE J.B. Iodine adsorption in metal organic frameworks in the presence of humidity, ACS Appl. Mater. Interfaces. **10**, 10622, **2018**.
2. ABDELMOATY Y.H., TESSEMA T.D., CHOUDHURY F.A., EL-KADRI O.M., EL-KADERI H.M., Nitrogen-rich porous polymers for carbon dioxide and iodine sequestration for environmental remediation, ACS Appl. Mater. Interfaces. **10**, 16049, **2018**.
3. HAN W., CLARKE W., PRATT S. Cycling of iodine by microalgae: iodine uptake and release by a microalgae biofilm in a groundwater-holding pond, Ecol. Eng. **94**, 286, **2016**.
4. MA Z., HAN Y., QI J., QU Z., WANG X. High iodine adsorption by lignin-based hierarchically porous flower-like carbon nanosheets, Ind. Crop. Prod. **169**, 113649, **2021**.
5. ZHANG T., YUE X., GAO L., QIU F., XU J., RONG J., PAN J. Hierarchically porous bismuth oxide/layered double hydroxide composites: preparation, characterization and iodine adsorption, J. Clean. Prod. **144**, 220, **2017**.
6. World Health Organization. *Iodine in drinking-water* (No. WHO/HEP/ECH/WSH/2020.5). World Health Organization (2020).
7. LUO Y., KAWASHIMA A., ISHIDO Y., YOSHIHARA A., ODA K., HIROI N., ITO T., ISHII N., SUZUKI K. Iodine excess as an environmental risk factor for autoimmune thyroid disease, Int. I. Mol. Sci. **15**, 12895, **2014**.
8. [8] SAKA C. YARDIM Y. ŞAHIN Ö. BAYTAR O. Iodine adsorption and electrochemical double-layer capacitor characteristics of activated carbon prepared from low-cost biomass. *Int. J. Phytoremediation*, **1**.
9. NENOFF T.M., RODRIGUEZ M.A., SOELBERG N.R., CHAPMAN K.W. Silver-mordenite for radiologic gas capture from complex streams: Dual catalytic CH3I decomposition and I confinement, Microporous Mesoporous Mater. **200**, 297, **2014**.
10. ZHOU J., LAN T., LI T., CHEN Q., BAI P., LIU F., YUAN Z., ZHENG W., LUO X., YAN W., YAN T. Highly efficient capture of iodine in spent fuel reprocessing off-gas by novelly porous copper-doped silica zeolites. Sep. Purif. Technol. **290,** 120895, **2022**.
11. SCOTT S.M., HU T., YAO T., XIN G., LIAN J. Graphene-based sorbents for iodine-129 capture and sequestration, Carbon. **90**, 1, **2015**.
12. SUBRAHMANYAM K.S., SARMA D., MALLIAKAS C., POLYCHRONOPOULOU K., RILEY B.J., PIERCE D.A., CHUN J., KANATZIDIS M.G., Chalcogenide aerogels as sorbents for radioactive iodine, Chem. Mater. **27**, 2619, **2015**.
13. ZHANG X., MADDOCK J., NENOFF T.M., DENECKE M.A., YANG S., SCHRÖDER M. Adsorption of iodine in metal-organic framework materials. Chemical Society Reviews. 8, **2022**.
14. XIE W., CUI D., ZHANG S.R., XU Y.H., JIANG D.L., Iodine capture in porous organic polymers and metal-organic frameworks materials, Mater. Horiz. **6**, 1571, **2016**.
15. YU X., YU Z.Y., ZHANG X.L., ZHENG Y.R., DUAN Y., GAO Q., WU R., SUN B., GAO M.R., WANG G., YU S.H. Superaerophobic nickel phosphide nanoarray catalyst for efficient hydrogen evolution at ultrahigh current densities, J. Am. Chem. Soc. **141**, 7537, **2019**.
16. SHAO L., LIU N., WANG L., SANG Y., ZHAN P., ZHANG L., HUANG J., CHEN J. Facile preparation of oxygen-rich porous polymer microspheres from lignin-derived phenols for selective CO_2 adsorption and iodine vapor capture. Chemosphere. **288**, 132499, **2022**.
17. BARMAN B.K., BARMAN S., ROY M.N. Inclusion complexation between tetrabutylphosphonium methanesulfonate as guest and α- and β-cyclodextrin as hosts investigated by physicochemical methodology, J. Mol. Liq. **264**, 80, **2018**.
18. SZENTE L., FENYVESI É., SZEJTLI J. Entrapment of iodine with cyclodextrins: potential application of cyclodextrins in nuclear waste management, Environ. Sci. Technol. **33**, 4495, **1999**.
19. DIAZ D., VARGAS-BACA I., GRACIA-MORA J. Beta-cyclodextrin inclusion complexes with iodine: An advanced and inexpensive undergraduate chemistry experiment, J. Chem. Edu. **71**, 708, **1994**.
20. HIROTA M., HIGAKI S., ITO S., ISHIDA Y., TERAO K. Radioactive iodine volatilization inhibition effect of cyclodextrin. J.l Radioanal. Nucl. Chem. **320** (3), 621, **2019**.
21. DEMBEK M., BOCIAN S., BUSZEWSKI B., Solvent Influence on Zeta Potential of Stationary Phase-Mobile Phase Interface. Molecules, **27** (3), 968, **2022**.
22. LIU Y., CHEN Y., GAO X., FU J., HU L. Application of cyclodextrin in food industry. Critical Reviews in Food Science and Nutrition, **62 (**10), 2627, **2022**.
23. MORENO-CASTILLA C., LÓPEZ-RAMÓN M.V., CARRASCO-MARÍN F. Changes in surface chemistry of activated carbons by wet oxidation, Carbon. **38**, 1995, **2000**.
24. American Society for Testing and Materials, Standard Test Method for Apparent Density of Activated Carbon: Designation: D2854-09, **2009**.
25. EL-SHAFEY E.I,. ALI S.N., AL-BUSAFI S., AL-LAWATI H.A. Preparation and characterization of surface functionalized activated carbons from date palm leaflets and application for methylene blue removal, J. Environ. Chem. Eng. **4**, 2713, **2016**.
26. BAILLOT R., DESHAYES Y. Tools and Analysis Methods of Encapsulated LEDs in: Reliability Investigation of LED Devices for Public Light Applications. 43, **2017**.
27. EL-SHAFEY E.S.I., AL-KITANI B.S. Comparative chemical analysis of some traditional Omani-made kohl, Toxicol. Environ. Chem. **99**, 233, **2017**.
28. AHMED M.O., SHRPIP A., MANSOOR M. Synthesis and characterization of new schiff base/thiol-functionalized mesoporous silica: an efficient sorbent for the removal of Pb (II) from aqueous solutions, Processes **8**, 246, **2020**.
29. ANBARASU G., MALATHY M., KARTHIKEYAN P., RAJAVEL R. Silica functionalized Cu (II) acetylacetonate Schiff base complex: An efficient catalyst for the oxidative condensation reaction of benzyl alcohol with amines, J. Solid State Chem. **253**, 305, **2017**.
30. YAO Y., LI Z., QIU Y., BAI J., SU J., ZHANG D., JIANG S. Unprecedented reactions: from epichlorohydrin to epoxyglycidyl substituted divinyl ether and its conversion into epoxyglycidyl propargyl ether, Sci. Rep-UK. **5**, 1, **2015**.
31. RAOF S.F.A., MOHAMAD S., ABAS M.R. Synthesis and evaluation of molecularly imprinted silica gel for 2-hydroxybenzoic acid in aqueous solution, Int. J. Mol. Sci. **14**, 5952, **2013**.
32. FIGUEIREDO J.L., PEREIRA M.F.R., FREITAS M.M.A., ORFAO J.J.M. Modification of the surface chemistry of activated carbons, Carbon. **37**, 1379, **1999**.

33. HIROTA M., HIGAKI S., ITO S., ISHIDA Y., TERAO K. Effects of 2-hydroxypropyl α-cyclodextrin on the radioactive iodine sorption on activated carbon, J. Radioanal. Nucl. Ch. **328**, 659, **2021**.
34. KAGHAZCHI T., KOLUR N.A., SABET R.H. Recovery of iodine with activated carbon from dilute aqueous solutions. AFINIDAD LXVI. **542,** 338, **2009**.
35. MARSH H., REINOSO F.R. Activated carbon, Elsevier. **2006**.
36. WEBER W.J., MORRIS J.C. Kinetics of adsorption on carbon from solution, J. Sanit. Eng. Div. **89**, 31, **1963**.
37. HO Y.S., MCKAY G. Sorption of dye from aqueous solution by peat, Chem. Eng. J. **70**, 115, **1998**.
38. LIAO Y., WEBER J., MILLS B.M., REN Z., FAUL C.F. Highly efficient and reversible iodine capture in hexaphenylbenzene-based conjugated microporous polymers, Macromolecules. **49**, 6322, **2016**.
39. LIU C., HUANG P.M. Kinetics of lead adsorption by iron oxides formed under the influence of citrate, Geochim. Cosmochim. Acta. **67**, 1045, **2003**.
40. HALL K.R., EAGLETON L.C., ACRIVOS A., VERMEULEN T. Pore-and solid-diffusion kinetics in fixed-bed adsorption under constant-pattern conditions, Ind. Eng. Chem. Fund. **5**, 212, **1966**.
41. JHA P.K., JHA V.K. Iodine adsorption characteristics of activated carbon obtained from Spinacia oleracea (spinach) leaves, Mongolian J. Chem. **21** (47), 1, **2020**.
42. XU L., ZHENG Q., WANG Y., JIANG L., JIANG J., QIU J. A pillared double-wall metal-organic framework adsorption membrane for the efficient removal of iodine from solution, Sep. Purif. Technol. **274**, 118436, **2021**.
43. SUKSOMPONG T., THONGMEE S., SUDPRASERT W., Efficacy of a graphene oxide/chitosan sponge for removal of radioactive iodine-131 from aqueous solutions, Life. **11**, 721, **2021**.
44. HUANG H., SHA X., CUI Y., SUN S., HUANG H., HE Z., LIU M., ZHOU N., ZHANG X., WEI Y. Highly efficient removal of iodine ions using MXene-PDA-Ag2Ox composites synthesized by mussel-inspired chemistry, J. Colloid Interf. Sci. **567**, 190, **2020**.